UV photodissociation of oxalyl chloride yields four fragments from one photon absorption

Musahid Ahmed, David Blunt, Daniel Chen, and Arthur G. Suits[a)]
Chemical Sciences Division, Ernest Orlando Lawrence Berkeley National Laboratory, Berkeley, California 94720

(Received 4 December 1996; accepted 6 February 1997)

The photodissociation of oxalyl chloride, $(ClCO)_2$, has been studied near 235 nm using the photofragment imaging technique. Observed products include both ground state Cl ($^2P_{3/2}$) and spin-orbit excited Cl*($^2P_{1/2}$) chlorine atoms and ground electronic state CO molecules. The rotational distribution obtained for the CO v=0 product is peaked at about J=30 and extends beyond J=50. Photofragment images were recorded for both chlorine atom fine structure components as well as many rotational levels of the CO v=0, yielding state-resolved angular and translational energy distributions. The recoil speed distribution for the Cl* exhibits a dominant fast component, with a translational energy distribution peaking at about 48 kJ/mol. The ground state chlorine atom showed two components in its speed distribution, with the slow component dominant. The corresponding translational energy distribution peaked at 10 kJ/mol but extended to 80 kJ/mol. The total average translational energy release into the Cl product is 34 kJ/mol. Similarly, the low rotational levels of the CO showed only a slow component, the intermediate rotational levels showed a bimodal speed distribution, and the highest rotational levels showed only the fast component. The fast components of both chlorine atom product and the higher rotational levels of the CO show an anisotropic angular distribution, while all slow fragments show a nearly isotropic angular distribution. These observations suggest a novel dissociation mechanism in which the first step is an impulsive three-body dissociation yielding predominantly Cl*, rotationally excited CO and chloroformyl radical ClCO, with only modest momentum transfer to the latter species. Most of the remaining ClCO undergoes subsequent dissociation yielding low rotational levels of CO and little translational energy release.
[S0021-9606(97)01418-9]

I. INTRODUCTION

When a photochemical event leads to the breaking of several chemical bonds, the timing of the bond scissions and the energy release to the fragments provide a window into the chemical dynamics underlying these unusual processes. This has motivated considerable interest and extensive study for such systems as s-tetrazine,[1] glyoxal[2–4] and acetone,[5–7] where absorption of a single photon can lead to three product fragments. To our knowledge, no reports have appeared to date for systems dissociating to four fragments following absorption of a single UV photon. The reason for this is simply that the energetics of breaking three bonds usually makes it impossible. Oxalyl chloride, $(ClCO)_2$, the chlorine-substituted analogue of glyoxal, possesses bond dissociation energies (D_o ClCO–ClCO=322 kJ/mol and D_o Cl–CO= 25 kJ/mol in ClCO)[8] such that dissociation into the four fragments Cl+Cl+CO+CO is possible at 235 nm with a further 167 kJ/mol available energy. All of the fragments, furthermore, can be detected via resonant multiphoton ionization (REMPI) in the vicinity of 235 nm. Oxalyl chloride is thus an ideal candidate for investigation of multiple bond-breaking processes via the photofragment imaging technique.[9,10]

The structure and conformational properties of oxalyl chloride have been the subject of a number of studies over the past forty years, owing to interest in the nature of the internal rotations about the carbon-carbon bond and the existence and identity of conformers beyond the lowest energy anti form.[11–14] Surprisingly, there have been no studies of oxalyl chloride photochemistry in the ultraviolet. One study reported the thermal decomposition of oxalyl chloride induced by a CO_2 laser, with detection of the reactant $(COCl)_2$ and product $COCl_2$ by infrared absorption.[15] The results were unaltered following addition of radical scavengers NO and propene, suggesting a concerted thermal decomposition: $(COCl)_2 \rightarrow CO+COCl_2$. The UV-induced photoisomerization of oxalyl chloride was studied in an argon matrix using Fourier-transform IR spectroscopy.[16] The authors found evidence of a *cis* form and interconversion between the *cis* and a *gauche* conformer. In addition, UV irradiation of oxalyl chloride in a xenon matrix led to the formation of CO and phosgene; however, this photochemical process was not the focus of the study and was not reported in detail.

A recent study using ion time-of-flight explored the photodissociation dynamics of phosgene,[17] a closely related system. In the phosgene study, both Cl and Cl* were detected, and both were found to exhibit bimodal translational energy distributions. The ground state chlorine atom distribution was found to be dominated by the slow component, while for

a)Author to whom correspondence should be addressed.

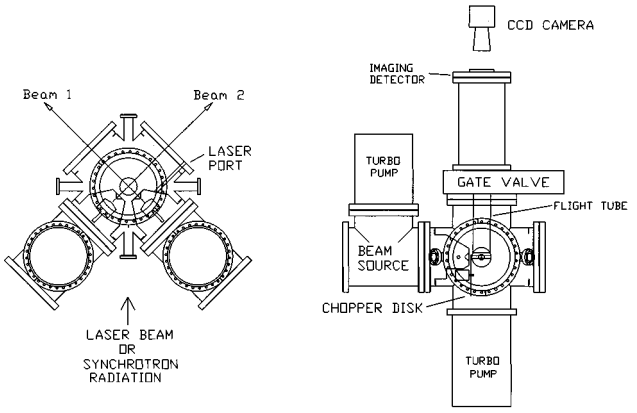

FIG. 1. Schematic view of ''universal imaging'' machine. Left view is from above, right view is into the primary beam source.

the Cl* both fast and slow components were of comparable magnitude. Based upon the translational energy distributions, the authors inferred a concerted three-body dissociation to Cl+Cl+CO in the phosgene case. Measurements of the CO internal state and translational energy distributions were not reported for that system.

We have undertaken a detailed study of the photochemistry of oxalyl chloride near 235 nm, measuring complete translational energy and angular distributions for all fragments with quantum state resolution, with an eye to exploring the detailed dynamics in this sytem capable of dissociation to four fragments following one-photon excitation. These experiments were performed in a new ''universal imaging'' crossed beam apparatus that has been constructed as a part of the Chemical Dynamics Beamline, a national user facility recently commissioned at the Advanced Light Source.[18,19]

II. EXPERIMENT

A. The ''universal imaging'' machine

As these represent the first experimental results obtained using the new ''universal imaging'' machine (so-called owing to the planned use in conjunction with tunable undulator VUV probe), some detail will be provided concerning the apparatus. The design is based on that of Houston *et al.*[20] and is shown schematically in Fig. 1. The main chamber is a modified six-way 12″ conflat cross, with four additional 2-3/4″ conflat ports at 45 deg to the main ports in one plane. Four keying rings have been welded just inside the four main ports, on which may be bolted the source differential cones. All components have been manufactured to key together so that there is no adjustment of the molecular beam sources. The differential cones are configured so that a mechanical chopper motor can be mounted to chop the molecular beam pulses to 5 microseconds or less, for future crossed-beam experiments or studies using the undulator radiation. The source regions have ports for access of lasers to the nozzle regions for photolytic radical production. The molecular beam sources, typically fixed at 90° but capable of operating in a counterpropagating configuration, are each pumped by 700 l/s high-throughput compound turbomolecular pumps (Osaka TG-703M), while the main chamber is pumped by a 1000 l/s magnetic bearing turbomolecular pump (Seiko-Seiki STP-1000). The latter pump is backed by an oil-free scroll pump (Galiso-Nuvac NDP-18HV) providing a completely oil-free system in the ionization region. The molecular beams cross at the center of the main chamber on the axis of a time-of-flight mass spectrometer. The products are ionized either by REMPI using UV lasers, or direct one-photon ionization using VUV undulator radiation typically introduced via the smaller ports at 45 deg. Product ions are accelerated by repeller and acceleration fields into a one meter flight tube perpendicular to the plane of the beams. Product ions strike the position-sensitive detector, which is an 80-mm diameter dual microchannel plate coupled to a phosphor screen (Galileo 3075FM). Mass-selected images were obtained by pulsing the microchannel plate, typically pulsing from a DC value of −1100 V to −1900 V, with 1 microsecond duration. The detector is viewed by an integrating fast-scan video camera system (Hammamatsu) employing thresholding in conjunction with a linear video look-up table. Future crossed-beam experiments will employ a custom-built video system capable of integration with 32-bit depth and operation at frame rates to 220 Hz (Data Design AC-101M) and linear or, in some cases a binary, look-up table for single ion accumulation. Typical accumulation times were 10 minutes for each image. Some of the images were re-recorded on a different apparatus, to be described in detail in a future publication.[21]

For the oxalyl chloride photodissociation studies, experiments were performed using a single molecular beam source and a single laser providing both dissociation and probe light (one-color experiments). The molecular beam was produced by bubbling helium through oxalyl chloride held at −10 °C, yielding a 3% beam. The mixture was expanded through a Proch-Trickl piezoelectric pulsed valve[22] operating at 30 Hz, with 150 microsecond pulses. The laser light was generated using a seeded Nd-Yag-pumped (Spectra-Physics GCR 290-30) dye laser (Laser Analytic Systems LDL) with a Bethune amplifier cell, operating with pyridine 1 around 700 nm. The laser light was first doubled in BBO, then the doubled light mixed with the fundamental to give the third harmonic of the dye. Polarization was adjusted with a half-wave plate before the first doubling crystal. Typical output power was 1-2 mJ/pulse at 30 Hz, and relatively constant throughout the tuning range from 225-235 nm. This configuration was found to give both a longer dye lifetime and broader tuning range when contrasted with doubling a 355 nm pumped dye. The laser linewidth was narrower than 0.04 cm^{-1} on the dye fundamental, so that it was necessary to scan across the Doppler width of the lines while each image was recorded.

Mass spectra were recorded by placing a photomultiplier tube to view the detector. REMPI scans of the CO were also recorded using the photomultiplier, with the signal fed into a boxcar averager gated on the mass of interest. REMPI (2+1) detection of Cl and Cl* was performed on numerous lines in the vicinity of 235 nm.[23] CO was detected by 2+1 REMPI

on the ($B \leftarrow X$) Q-branch transition at 230 nm.[24] The scans were conducted under conditions with sufficent averaging that the laser power was constant ($\pm 5\%$), so that no correction for laser power was necessary. The relative populations were obtained from the simulations discussed below following correction for the appropriate line strength factor (2J $+1$)/9.

The images recorded are 2-dimensional projections of the 3-dimensional recoiling product sphere. The translational energy and angular distributions are reconstructed from the projection using standard techniques.[10] In all cases presented here the translational energy distributions are reported for each fragment separately, since there are 3-body processes involved that do not conserve linear momentum between any two fragments.

III. RESULTS

These experiments represent one-color studies of the photodissociation of oxalyl chloride at numerous wavelengths in a narrow range. As such, the photolysis wavelength changes slightly with the species probed. Since the absorption spectrum is not discrete in this region it is assumed, as is commonly done,[17,25] that small changes in the available energy do not dramatically influence the dissociation dynamics. This is not always the case, even for systems lacking a discrete absorption spectrum.[26] However, the availability of several lines for Cl and Cl* provided a valuable check on this assumption. Both translational energy and angular distributions for the chlorine atom products were insensitive to the particular state probed, confirming both that the dynamics do not change rapidly with wavelength in this region, and that orbital alignment of the chlorine atom, if present, is not influencing the measured distributions. Multiphoton dissociation processes may be ruled out since the additional 500 kJ/mol would appear in the translational and rotational energy distributions shown below.

A. Chlorine atom translational energy distributions

Images recorded for the spin-orbit excited (Cl*($^2P_{1/2}$)) and ground state (Cl ($^2P_{3/2}$)) chlorine atoms are shown in Figs. 2(a) and (b), respectively. The corresponding translational energy distributions ($P(E_T)$'s) extracted from the images are shown in Fig. 3. The Cl* $P(E_T)$ shows a dominant fast (i.e., high E_T) component peaking at 48 kJ/mol, with an average of 47 and a full width at half-maximum of 38 kJ/mol. A small (8%) contribution from a ''slow'' component is also present. The translational energy distributions were fitted as two components, shown as dashed lines in the figure. The slow component peaks at 10 and extends to 80 kJ/mol with an average of 22 kJ/mol. This component was fitted with the expression $P(E_T)=(E_{col}-E_{exo})^P*(E_{exo}-B)^Q$, often used to describe the statistical decomposition of a collision complex, using the parameters $E_{col}=$ 28.9 kJ/mol, P=0.4, Q=5.4 and B=-2 kJ/mol and E_{exo}=86 kJ/mol. No direct physical significance is ascribed to these parameters, however. A Gaussian was employed to fit the ''fast'' component. The latter peaks at 48 kJ/mol with an average of 47 kJ/mol. The fit yields 22% of the fast component for the ground state Cl, though the fraction could vary considerably with the choice for the description of the slow component. The $P(E_T)$ for the ground state Cl atom is shown in Fig. 3. In contrast to the Cl*, the Cl $P(E_T)$ is dominated by the slow component. The ground state Cl also shows a contribution from the ''fast'' component, shown as a dot-dash line in Fig. 3. The bimodal nature of the distribution is more apparent in the speed distributions rather than the translational energy distributions, but the justification for fitting it as two components is further shown in the angular distributions below. These ''slow'' and ''fast'' components used to fit the experimental results are identical for both the Cl* and Cl, only the relative contributions have been varied in each case.

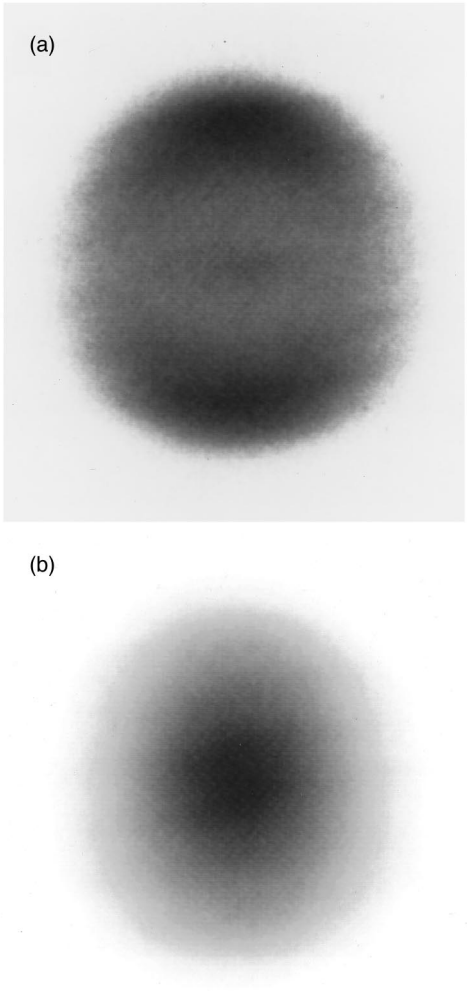

FIG. 2. (a). Raw image of Cl*($^2P_{1/2}$) recorded with dissociation and probe at 235.205 nm on the $4p^2P_{1/2} \leftarrow\leftarrow 3p^2P_{1/2}$ transition. (b) Raw image of Cl($^2P_{3/2}$) recorded with dissociation and probe at 235.336 nm on the $4p^2D_{3/2} \leftarrow\leftarrow 3p^2P_{1/2}$ transition. The laser polarization direction is vertical in the plane of the images.

B. Chlorine atom angular distributions

The chlorine atom angular distributions derived from the images are shown in Fig. 4. The Cl* angular distribution is clearly anisotropic, yielding an anisotropy parameter $\beta=$

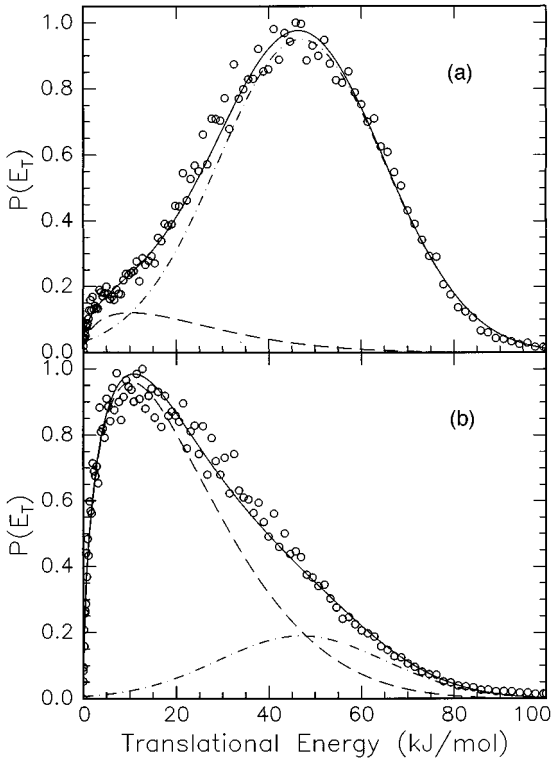

FIG. 3. Chlorine atom center-of-mass translational energy distributions obtained from the images in Fig. 2. Circles are experimental points and lines are results of fit as described in text. (a) Cl*($^2P_{1/2}$). (b) Cl($^2P_{3/2}$).

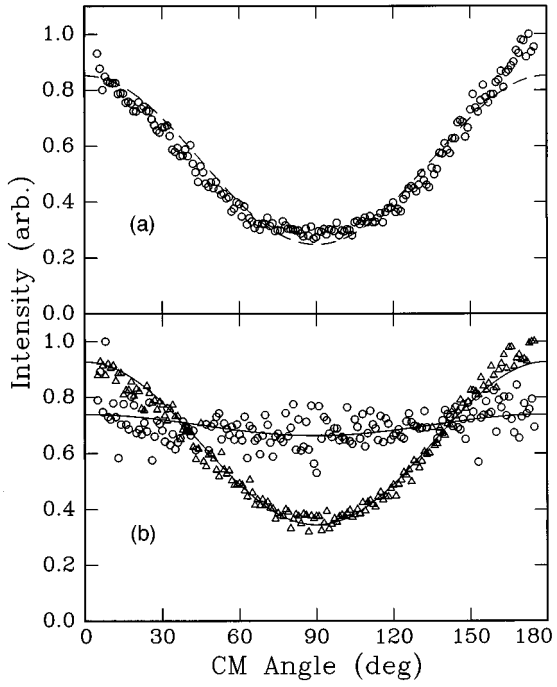

FIG. 4. Chlorine atom angular distributions obtained from the images in Fig. 2. (a) Cl*($^2P_{1/2}$). Circles are experimental points and the line is the fit yielding $\beta=0.7$ (b) Cl($^2P_{3/2}$). Circles are experimental points below 1000 m/s (18 kJ/mol), ''slow component'', and line is fit yielding $\beta=0.07$. Triangles are experimental points above 1000 m/s (18 kJ/mol), ''fast component'', and solid line is fit yielding $\beta = 0.9$.

0.89, where the β parameter describes the angular distribution via the well-known expression: $I(\theta)=(1/4\pi)[1+\beta(P_2(\cos(\theta))]$.[27] The reconstruction technique accumulates the noise in the image into the center strip, so that the results near the poles are always associated with larger error bars. The angular distribution for the ground state chlorine atom are shown in Fig. 4(b). Two different angular distributions are shown: one corresponding to the total contribution below 18 kJ/mol translational energy, the other represents the total above 18 kJ/mol. The faster component shows a substantially more polarized angular distribution, in fact quite close to that of the Cl*. The β values obtained are 0.07 for the slow fraction and 0.72 for the fast component.

C. Branching fractions

The branching into the different distributions for the Cl and Cl* are summarized in Table I. The relative contributions for the Cl and Cl* were obtained by scaling the integrated REMPI signals using the relative line strengths for detection of Cl* at 237.808 nm (''a,'' $4p^2P_{1/2}\leftarrow\leftarrow 3p^2P_{1/2}$) and 235.205 nm (''b,'' $4p^2D_{3/2}\leftarrow\leftarrow 3p^2P_{1/2}$) with that for Cl at 235.336 nm (''c,'' $4p^2D_{3/2}\leftarrow\leftarrow 3p^2P_{3/2}$). Published values for the relative line strengths are 2.5 ± 0.1 for c/a and 0.8 ± 0.1 for c/b.[28–31] Alternative values of 1.8 and 0.6 are obtained for c/a and c/b based on recent measurements of the Cl/Cl* branching ratio in HCl by Wittig and co-workers.[32] In addition to the spin-orbit branching, yielding 36% Cl*, the distributions are further subdivided according to the relative amounts of fast and slow components, obtained via the fit to the ground state distribution discussed above. The result gives very close to half-and-half fast and slow Cl atom product, with the bulk of the fast Cl appearing as Cl*. These branching fractions are summarized in Table I, with the overall results for the average energy release and β parameters summarized in Table II.

D. REMPI spectrum of CO

The REMPI spectrum for the CO v=0 product is shown in Fig. 5(a), along with a simulation. The isolated peak near the Q-branch bandhead is well-fitted with a rotational temperature of 300 K, and represents background CO. The v=1 distribution (not shown) is not rotationally resolved and is not quantified in this study. However, the total integrated intensity of the (1-1) band was less than 5% that of the (0-0) band, implying the predominance of the v=0 component despite the uncertainty in the Franck-Condon factors and other

TABLE I. Branching in Cl photofragments. See text for discussion of ''fast'' and ''slow'' components. Values in percent. Values in parentheses are obtained based on a revised value for the spin-orbit branching ratio in HCl at 193 nm (Ref. 32).

	Slow	Fast	Total
Cl	50(56)±7	14(15)±7	64(71)±10
Cl*	2(2)	34(27)±10	36(29)±10
Total	52(58)±10	48(42)±10	

TABLE II. Energy release and β parameters.

	$\langle E \rangle$ (kJ/mol)	β
Cl (slow)	22.1	0.07
Cl (fast)	47.2	0.72
Cl (total)	27.4	
Cl* (slow)	22.1	
Cl* (fast)	47.2	0.89
Cl* (total)	45.0	0.89
Cl+Cl*	33.8	
CO (v=0, J=22)	12.3	0.04
CO (v=0, J=30)	29.9	−0.03 (slow) 0.41 (fast)
CO (v=0, J=55)	30.3	0.45

aspects of the relative transition strength. The simulation was used to extract the rotational distribution of the CO v=0, shown in Fig. 5(b). The distribution peaks at J=28, with levels as low as 15 and beyond 50 populated. It was necessary to include a J-dependent width of the lines in the simulation owing to the broadening of the Doppler width at high J (see below).

E. State-resolved CO images

Images corresponding to three different representative J levels of the CO ground vibrational level are shown in Fig. 6, and the energy distributions extracted from the images are shown in Fig. 7. These images were obtained by scanning across the corresponding rotational lines of Fig. 5 at the indicated wavelength. As can be clearly seen in both figures, the energy distributions change dramatically with J: for low J (J=22), the translational energy release is relatively low,

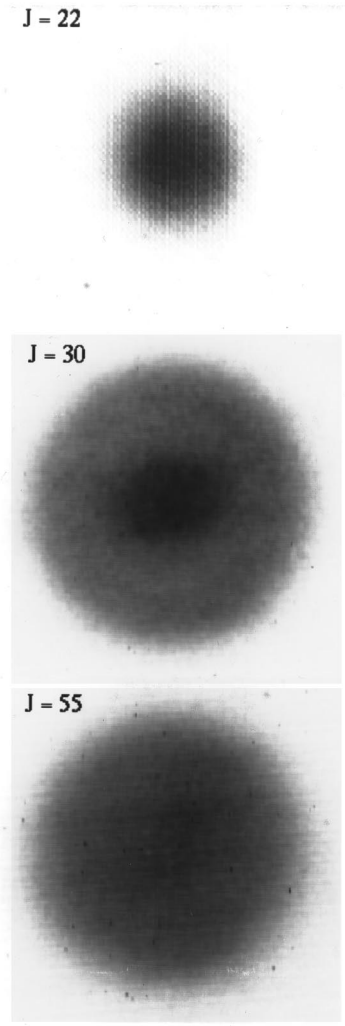

FIG. 6. Photofragment images for indicated rotational levels of CO v=0.

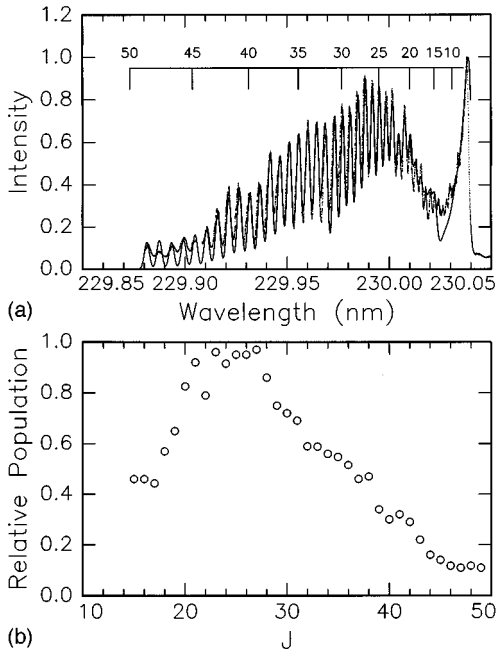

FIG. 5. (a) REMPI scan of CO v=0 on the $B \leftarrow\leftarrow X$ transition obtained as described in text (+), along with simulation (solid line). (b) Rotational population obtained from the simulation above.

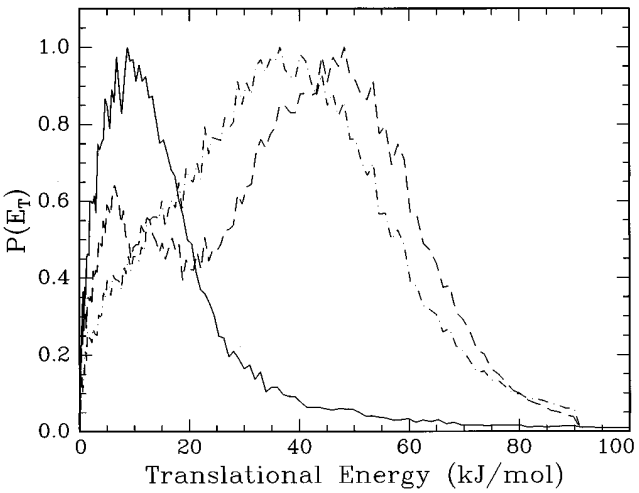

FIG. 7. Translational energy distributions for CO (v=0,J) obtained from the preceding 3 images. Solid line, J=22; dot-dash, J=30; dashed, J=55.

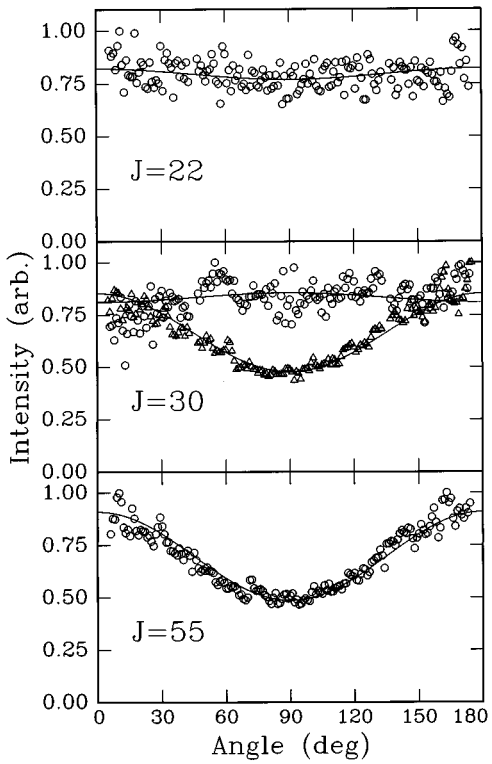

FIG. 8. Center-of-mass angular distributions for the indicated rotational levels of CO v=0, obtained from the images in Fig. 6. For J=30, the two curves represent those CO molecules recoiling less than 1000 m/s (''slow'') or faster than 1000 m/s (''fast'').

peaking at about 8 and extending beyond 60 kJ/mol. At intermediate values, the translational energy distributions are clearly bimodal, further suggesting a relation to the chlorine atom distributions. At high J, the fast component is dominant, with the translational energy release peaking at about 40 kJ/mol. The nature of the distributions appeared to change fairly smoothly as a function of J, with no sudden variations in the relative amounts of the slow and fast components. Angular distributions for these three rotational levels are shown in Fig. 8. A single beta value is extracted from the J=22 (β=0.04) and J=55 (β=0.45) data, although the J=22 may include some contribution from a distinct fast component. The J=30 result clearly consists of two components, and distinct beta values are obtained for the slow and fast portions of the distribution, somewhat arbitrarily set at 34 kJ/mol. Just as in the Cl case, the slow component is nearly isotropic (β=−0.03) while the fast component shows significant anisotropy (β=0.41).

F. Vector correlations

Photofragment imaging can be a sensitive probe of vector correlations in the dissociation process, both for correlation between the recoil direction and the rotational angular momentum,[33,34] and between the recoil direction and atomic orbital alignment.[35] Such vector correlations can impact the inferred angular distributions if they are present yet unaccounted for. It should be emphasized that if the dissociation and probe lasers are parallel, the translational energy distributions are not affected even if unknown vector correlations are present, so long as the angular and translational energy distributions are uncoupled. This is because cylindrical symmetry is preserved, so the inverse Abel transformation used to reconstruct the distribution remains valid. It is not straightforward to investigate these phenomena in one-laser experiments, since the polarization of the probe and dissociation laser cannot be varied independently. However, Sato *et al.* have shown that the (B-X) Q-branch transition in CO is insensitive to vector correlations.[25] **v-J** correlations may indeed be present in the CO product, but the present experiment is not sensitive to them.

Alignment of the chlorine atom atomic orbital is possible, however,[36,35] and could impact the observed angular distributions. The strongest evidence that unknown orbital alignment is not dramatically influencing the observed distributions is that the same angular distributions are seen on numerous different transitions in this vicinity. Given atomic orbital alignment in the product, differing transitions would, in general, show clearly different behavior.

IV. DISCUSSION

These distributions suggest a simple picture of the dissociation dynamics. Because we find Cl and CO fragments that are near momentum-matching, it seems clear that they are dynamically linked. However, the only way to obtain free Cl and CO in a single step is to break both the C-C and the Cl-CO bonds simultaneously. Furthermore, at the same time we must end up with another population of Cl and CO that possesses little translational energy, since there is a similar momentum-matching pair that shows little recoil speed and an isotropic angular distribution. For this to occur, the C–C bond scission must take place with little concomitant momentum transfer to the remaining chloroformyl radical, yet with transfer of sufficient internal energy to break the Cl–CO bond in the radical. This process is schematically illustrated in Fig. 9. The initial step breaking the C–C bond and one of the Cl–CO bonds takes place with an impulse more-or-less along the Cl–CO bond axis. The C–C bond must break simultaneously to preclude coupling of a substantial portion of this impulse to the remaining fragments. The initial impulse yields fast, rotationally excited CO and Cl that is predominantly (72%) in the spin-orbit excited state. However, a portion of the fast Cl is formed in the ground state.

This simple model has several implications that can readily provide a rough check on its validity. The first point is that since we have state-resolved translational energy distributions for representative examples of all fragments, we can roughly verify the energy balance. Although we have not obtained full translational energy distributions for all CO rotational levels, we do have the rotational distribution for v=0, clearly the principal vibrational level. Furthermore, if we use the $P(E_T)$ for the dominant rotational levels to represent the total distribution we will not be led too far astray, since they contain contributions from the fast and slow components that dominate the higher and lower J levels, respec-

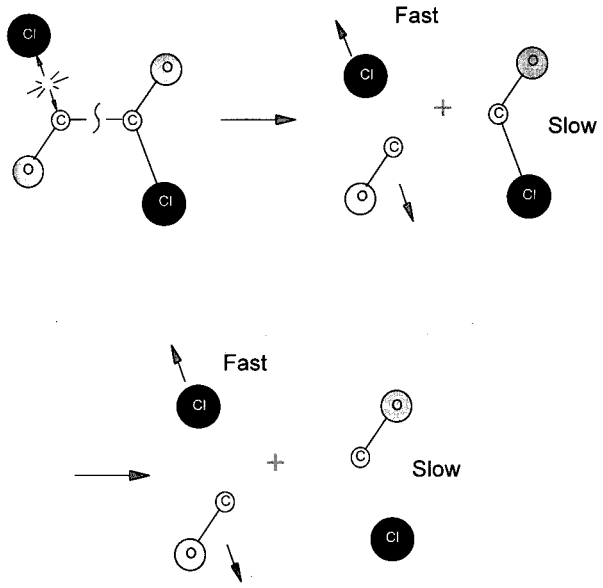

FIG. 9. Cartoon representation of the dissociation model (see Discussion).

tively. We can thus obtain the average energy in translation for all fragments. These are summarized in Table III. We obtain the average energy in rotation from the rotational distribution in Fig. 5. We neglect what we suspect are minor contributions from vibrationally excited CO. A small contribution from the electronic excitation is also included. In addition, the C–C bond energy and twice the Cl–CO bond in chloroformyl radical are also included. The total is compared to the photon energy at 235 nm. The rough agreement indicates that the mechanism is at least reasonable, and none of the products likely arise from processes involving another photon. The fact that our estimated energy release is a bit larger (531 vs. 509 kJ/mol) could be accounted for if some of the ClCO remains bound. Attempts to find the radical through ionization in this wavelength region were unsuccessful, but future studies will seek to quantify it as a primary product using alternative detection methods.

An alternate model to explain the bimodal distributions would involve invoking two distinct electronic states, or at least two different dissociation paths, with one showing prompt dissociation dynamics and the other perhaps following internal conversion and decomposition on the ground state to yield the slower product. Although the arguments are somewhat indirect, we find this picture unsatisfying for several reasons. The most important reason is that for both the slow and the fast atomic chlorine product, we find near-momentum-matching CO. As noted above, this requires simultaneous breaking of both the Cl–C and C–C bonds in the parent molecule. This leads directly to the picture we have outlined, unless it is argued that some events give exclusively fast products, while others give exlusively slow products. But any model that would give four fast fragments or four slow fragments, even for a portion of the dissociation events, would not conserve energy.

The nature of the electronic transition is not known here, and it may be related to the somewhat puzzling case of acetyl halides.[37,38,7,39] All of the acetyl halides show a parallel dissociation, with β values for the Cl product similar to those reported here. This is surprising since it is generally believed that the transition is an $n\rightarrow\pi^*$ transition, with the transition dipole expected to be perpendicular to the molecular plane. It has been argued that the upper state for acetyl chloride may be pyramidal, so that the out-of-plane transition moment might still yield a positive β owing to geometry changes in the decaying molecule. The more commonly invoked explanation for these positive β values is that the $n\rightarrow\pi^*$ transition may be coupled to an $n\rightarrow\sigma^*$ transition that is repulsive along the Cl–C axis. We are more comfortable with the latter picture, particularly since this behavior seems so widespread, and is relatively insensitive to the identity of the molecule and the dissociation wavelength.

TABLE III. Energy balance (kJ/mol). Photon energy at 235 nm is 509 kJ/mol.

C–C		322
Cl–CO	2×25	50
E_{trans}:		
Cl	2×33.8	67.6
CO	2×30	60
E_{rot}	2×14.2	28.4
E_{el}	2×3.5	7
Total		535

V. CONCLUSION

We have studied the detailed photodissociation dynamics of oxalyl chloride near 235 nm using the photofragment imaging technique. Observed products include both ground state Cl ($^2P_{3/2}$) and spin-orbit excited Cl*($^2P_{1/2}$) chlorine atoms and ground electronic state CO molecules. Quantum state resolved translational energy and angular distributions were obtained for representative examples of all fragments. These distributions suggest a novel dissociation mechanism in which the first step is an impulsive three-body dissociation yielding predominantly Cl*, rotationally excited CO and chloroformyl radical ClCO, with only modest momentum transfer to the latter species. Most, if not all, of the remaining chloroformyl radical subsequently dissociates, yielding low rotational levels of CO and little translational energy release.

ACKNOWLEDGMENTS

The authors are grateful to J. Zhang, M. Dulligan and C. Wittig for providing the revised value of the HCl spin-orbit branching ratio prior to publication, and thank C. Knopf for technical assistance. This work was supported by the Director, Office of Energy Research, Office of Basic Energy Sciences, Chemical Sciences Division of the U. S. Department of Energy under contract No. DE-ACO3-76SF00098.

[1] X. Zhao, W. B. Miller, E. J. Hintsa, and Y. T. Lee, J. Chem. Phys. **90**, 5527 (1989).
[2] J. Hepburn, R. Buss, L. Butler, and T. Lee, J. Phys. Chem. **87**, 3638 (1983).
[3] I. Burak, J. W. Hepburn, N. Sivakumar, G. E. Hall, G. Hall, and P. L. Houston, J. Chem. Phys. **86**, 1258 (1987).
[4] G. Scuseria and H. S. III, J. Am. Chem. Soc. **111**, 7761 (1989).
[5] K. A. Trentelman, S. H. Kable, D. B. Moss, and P. L. Houston, J. Chem. Phys. **91**, 7498 (1989).
[6] G. E. Hall, D. V. Bout, and T. J. Sears, J. Chem. Phys. **94**, 4182 (1991).
[7] S. W. North, D. A. Blank, J. D. Geseltzer, C. A. Longfellow, and Y. T. Lee, J. Chem. Phys. **102**, 4447 (1995).
[8] L. Walker and H. Prophet, J. Trans. Faraday Soc. **63**, 879 (1967).
[9] D. W. Chandler and P. L. Houston, J. Chem. Phys. **87**, 1445 (1987).
[10] B. J. Whitaker, in *Research in Chemical Kinetics Vol. 1*, edited by R. G. Compton and G. Hancock (Elsevier, Amsterdam, 1993).
[11] B. Saksena and R. Kagarise, J. Chem. Phys. **19**, 99 (1951).
[12] D. Hassett, K. Hedberg, and C. Marsden, J. Phys. Chem. **97**, 4670 (1993).
[13] D. Danielson, L. Hedberg, K. Hedberg, K. Hagen, and M. Trae, J. Phys. Chem. **99**, 9374 (1995).
[14] J. Durig, J. Davis, and A. Wang, J. Mol. Struct. **375**, 67 (1996).
[15] J. Pola, Collec. Czech. Chem. Comm. **47**, 3258 (1982).
[16] W. Schroeder, M. Monnier, G. Davidovics, A. Allouche, P. Verlaque, J. Pourcin, and H. Bodot, J. Mol. Struct. **197**, 227 (1989).
[17] C. Maul, T. Has, K.-H. Gericke, and F. Comes, J. Chem. Phys. **102**, 3238 (1995).
[18] P. A. Heimann, M. Kolke, C. W. Hsu, M. Evans, C. Y. Ng, X. M. Yang, C. Flaim, A. G. Suits, and Y. T. Lee, SPIE Proc. **2856**, 90 (1996).
[19] X. Yang, D. A. Blank, J. Lin, P. A. Heimann, A. M. Wodke, Y. T. Lee, and A. G. Suits, in *Synchrotron Radiation Techniques in Industrial, Chemical, and Materials Science*, edited by D'Amico *et al.* (Plenum, New York, 1996).
[20] L. S. Bontuyan, A. G. Suits, P. L. Houston, and B. J. Whitaker, J. Phys. Chem. **97**, 6342 (1993).
[21] D. A. Blunt and A. G. Suits (unpublished).
[22] D. Proch and T. Trickl, Rev. Sci. Instrum. **60**, 713 (1989).
[23] S. Arepalli, N. Presser, D. Robie, and R. J. Gordon, Chem. Phys. Lett. **118**, 88 (1985).
[24] G. Loge, J. Tiee, and F. Wampler, J. Chem. Phys. **79**, 196 (1983).
[25] Y. Sato, Y. Matsumi, M. Kawasaki, K. Tsukiyama, and R. Bersohn, J. Phys. Chem. **99**, 16307 (1995).
[26] J. A. H. M. A. Thelen, T. Gejo, and J. R. Huber, J. Chem. Phys. **103**, 7946 (1995).
[27] R. A. Zare and D. R. Herschbach, Proc. IEEE **51**, 173 (1963).
[28] Y. Matsumi, P. K. Das, and M. Kawasaki, J. Chem. Phys. **97**, 5261 (1992).
[29] J. Cao, H.-P. Loock, and C. X. W. Qian, Can. J. Chem. **72**, 758 (1993).
[30] R. Liyanage, Y. Yang, S. Hashimoto, R. Gordon, and R. W. Field, J. Chem. Phys. **103**, 6811 (1995).
[31] V. Skorokhodov, Y. Sato, K. Suto, Y. Matsumi, and M. Kawasaki, J. Phys. Chem. **100**, 12321 (1996).
[32] J. Zhang, M. Dulligan, and C. Wittig (unpublished).
[33] J. W. Thoman, D. W. Chandler, D. H. Parker, and M. H. M. Janssen, Laser Chem. **9**, 27 (1988).
[34] A. G. Suits, R. L. Miller, L. S. Bontuyan, and P. L. Houston, J. Chem. Soc. Faraday Trans. **89**, 1443 (1993).
[35] Y. Mo, H. Katayanagi, M. C. Heaven, and T. Suzuki, Phys. Rev. Lett. **77**, 830 (1996).
[36] Y. Wang, H.-P. Loock, J. Cao, and C. Qian, J. Chem. Phys. **102**, 808 (1995).
[37] M. D. Person, P. W. Kash, and L. J. Butler, J. Phys. Chem. **96**, 2021 (1992).
[38] M. D. Person, P. W. Kash, and L. J. Butler, J. Chem. Phys. **97**, 355 (1992).
[39] I. C. Lane, R. Meehan, and I. Powis, J. Phys. Chem. **99**, 12371 (1995).